Active vibration control of a flexible link robot with the use of piezoelectric actuators

Darren Williams[1,*], *Hamed* Haddad Khodoparast[1], and *Chenyuang* Yang[1]

[1]College of Engineering, Bay Campus, Swansea University, Wales, UK.

Abstract. Within robot systems the use of flexible links could solve many issues raised by their rigid counterparts. However, when these flexible links are integrated within systems which include moving parts their main issue lies in the vibrations experienced along their length due to disturbances. Much research effort has been made to solve this issue, with particular attention being paid to the application of piezoelectric patches as actuators within active vibration control (AVC). The study will consist of accurate models of a flexible link and two surface bonded piezoelectric patches, where the link and the piezoelectric patches will be modelled through the use of Euler-Bernoulli beam theory (EBT). The link will be subject to an initial displacement at its free end, and the resulting displacement of this end of the beam is to be controlled using a classic proportional-differential (PD) controller. The voltages to be applied across each of the actuators is to be controlled in accordance with the displacement of the free end of the beam, the actuators will then induce a strain upon the link opposing the movement of the tip. This research outlines this general method, obtains the best location of the piezoelectric patches and the control gains to be used, and proves that the method can be used to attenuate the vibrations experienced by a flexible link.

1 Introduction

The attenuation of unwanted vibrations is a popular topic within engineering research as multiple fields suffer from the issue when designing, manufacturing and implementing a multitude of designs. The issue affects the majority of the fields of engineering wherein designs include moving parts or are subject to uncontrollable external forces.

Within robotics active vibration control (AVC) is a prevalent area of research as most robot systems will contain moving parts which will be subject to unwanted vibrations. Flexible links within said systems are especially susceptible to unwanted vibrations, even more so than their rigid counterparts. However, the advantages of using flexible links opposed to rigid links greatly outweigh this disadvantage. Flexible links are easier to incorporate into a design, less expensive, and most importantly lighter. Having a system or design which is lighter overall is a highly sought property especially within the fields of robotics and aerospace where payload is a priority.

This leads to research becoming focussed on the AVC of these flexible links. The use of piezoelectric transducers as actuators and sensors has multiple advantages. The application of piezoelectric patches is non-intrusive to a design in the sense that the weight and functionality of said design will not be affected significantly. These lightweight components have a relatively high force output in comparison to their size, and can either be bonded to the surface or embedded within a component.

Crawley and Luis [1] were one of the first to suggest the use of piezoelectric actuators as elements of intelligent structures. They presented analytical models based on the Euler-Bernoulli theory (EBT) for long, slender beams, as well as physical experimentation. *Rathi and Khan* [2] compared the use of surface bonded and embedded piezoelectric actuators, as well as single input single output (SISO) and multiple input multiple output (MIMO) systems. *Nor et al.* [3] employed a proportional integral derivative (PID) controller to alter the voltage across a piezoelectric actuator in accordance with the transverse velocity at the location of the actuator on a plate. With the PID controller being designed within MATLAB® and implemented within COMSOL Multiphysics® via LiveLink™ for MATLAB®. *Wang and Wang* [4] presented their findings on the optimal placements and sizes of a collocated actuator pair surface bonded onto a beam. *Salmasi et al.* [5] produced an analytical model of a flexible link with surface bonded actuators and used simulation software to validate the analytical results through the comparison of the natural frequencies.

Within this research an analytical model of a flexible link with collocated piezoelectric actuators has been created using EBT. A model of the link has then been created within COMSOL Multiphysics® with the same dimensions and properties for the validation of the analytical results. A proportional-differential (PD) controller has been designed and implemented within the

* Corresponding author: 708199@swansea.ac.uk

analytical model. A parametric study has been conducted to obtain the best locations of the piezoelectric actuators and the optimal control gains, and these values have been implemented within the analytical model.

2 Modelling the flexible link

2.1 Description and analytical model

The flexible link and bonded piezoelectric actuator patches have been modelled mathematically as a beam based on the Euler-Bernoulli beam theory, as the link has dimensions which conform to those for which the theory holds (a long slender beam). The link is of length *L*, width *W*, thickness *T* and cross-sectional area *A*, and has Young's Modulus *E*, density ρ and a second moment of area I_x. The bonded piezoelectric patch has the same variables, but those corresponding to the patch are denoted through the subscript p. Fig.1 is a visual representation of the model, where *w(x,t)* represents the transverse motion of the link, and x_1 and x_2 represent the start and end locations, respectively, of the piezoelectric patches along the *x* axis. The bond between the piezoelectric patch and the link has been considered as perfect for this analytical model.

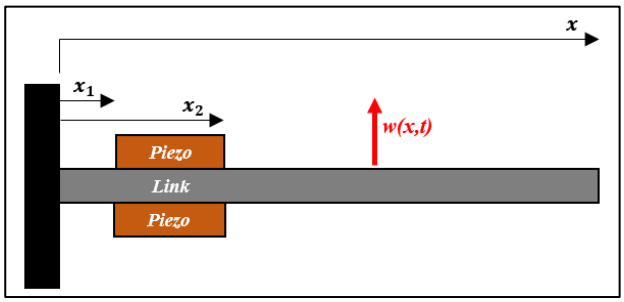

Fig. 1 Visualisation of the model

The equation of motion for the flexible link with a bonded piezoelectric actuator can be written as [6]:

$$\frac{\partial^2}{\partial x^2}\left(EI(x)\frac{\partial^2 w(x,t)}{\partial x^2}\right)+\rho A(x)\frac{\partial^2 w(x,t)}{\partial t^2} +c_a\frac{\partial w(x,t)}{\partial t}=F_0\sin(\Omega t)\,\delta(x-L) +\vartheta V sin(\Omega_V t)\left(\frac{d\delta(x-x_1)}{dx}-\frac{d\delta(x-x_2)}{dx}\right) \quad (1)$$

where, c_a is the viscous air damping coefficient, F_0 is the force applied to the structure and Ω and Ω_V are the frequencies of the force and the voltage applied within the model, respectively. As the density and Young's Modulus of the structure varies over its length, $EI(x)$ and $\rho A(x)$, are functions which vary with respect to *x* (see equations 2 and 3). The Dirac delta function is denoted as $\delta(x)$, and ϑ is the piezoelectric coupling term and can be calculated using equation 4 [7].

$$\rho A(x) = \rho A + \rho_p A_p[H(x-x_1)-H(x-x_2)] \quad (2)$$

$$EI(x) = EI_x + E_p I_{x_p}[H(x-x_1)-H(x-x_2)] \quad (3)$$

$$\vartheta = \frac{\bar{e}_{31}W}{20T_p}\left[\left(T_p+\frac{T}{2}\right)^2-\frac{T^2}{4}\right] \quad (4)$$

Within equations 2, 3 and 4 the Heaviside function has been denoted as *H(x)* and $\bar{e}_{31}$ is the effective transverse piezoelectric coefficient. The model is subject to the boundary conditions of a clamped-free beam.

Substituting equations 2 and 3 into equation 1, and employing the product rule yields:

$$\frac{\partial^2 EI(x)}{\partial x^2}\frac{\partial^2 w(x,t)}{\partial x^2}+2\frac{\partial EI(x)}{\partial x}\frac{\partial^3 w(x,t)}{\partial x^3} +EI(x)\frac{\partial^4 w(x,t)}{\partial x^4}+\rho A(x)\frac{\partial^2 w(x,t)}{\partial t^2} +c_a\frac{\partial w(x,t)}{\partial t}=F_0\sin(\Omega t)\,\delta(x-L) +\vartheta V sin(\Omega_V t)\left(\frac{d\delta(x-x_1)}{dx}-\frac{d\delta(x-x_2)}{dx}\right) \quad (5)$$

2.2 Reduced order model

The reduction of the order of the model requires the employment of the Galerkin Decomposition method [8]. Within this method the spatial dependence is eliminated though the substitution of the transverse motion of the link for a series expansion in terms of the eigenfunctions of the model. For the n^{th} mode the transverse motion can be expressed as:

$$w(x,t)=\sum_{n=1}^{N}T_n(t)X_n(x) \quad (6)$$

where, $T_n(t)$ is the n^{th} generalised coordinate, and $X_n(x)$ is the n^{th} mode shape of the link. Assuming single mode excitation (n^{th} mode) and using the Galerkin method yields:

$$M\ddot{T}_n(t)+C\dot{T}_n(t)+KT_n(t) = F_b\sin(\Omega t)+\theta_P V sin(\Omega_V t) \quad (7)$$

where,

$$M = \rho A(x)\int_0^L X_n^2(x)dx \quad (8)$$

$$C = c_a\int_0^L X_n^2(x)dx \quad (9)$$

$$K=\int_0^L\left[\frac{\partial^2 EI(x)}{\partial x^2}X_n''(x)+2\frac{\partial EI(x)}{\partial x}X_n'''(x) +EI(x)X_n^{iv}(x)\right]X_n(x)dx \quad (10)$$

$$F_b = F_0\int_0^L X_n(x)\delta(x-L)dx \quad (11)$$

$$\theta_p=\vartheta\left(\frac{dX_n(x_2)}{dx}-\frac{dX_n(x_1)}{dx}\right) \quad (12)$$

To solve for the generalised coordinate $T_n(t)$ Equation 7 can be rewritten as:

$$\ddot{T}_n(t) + 2\zeta\omega_n\dot{T}_n(t) + \omega_n^2 T_n(t) = F\sin(\Omega t) + \chi V sin(\Omega_V t) \quad (13)$$

where,

$$\zeta = \frac{C}{2M\omega_n}, \quad \omega_n = \sqrt{\frac{K}{M}}, \quad F = \frac{F_b}{M}, \quad \chi = \frac{\theta_p}{M}. \quad (14)$$

2.3 Validation

The simulation software COMSOL Multiphysics® was employed along with its MEMS module and the LiveLink™ for MATLAB® interface to create a finite element (FE) model of the link and the two piezoelectric patches for comparison with the analytical counterpart. The LiveLink™ for MATLAB® interface was used to control input variables and the computation of the COMSOL® model from the MATLAB® script. Thus, the results were returned from the simulation within the MATLAB® desktop, which ensured easier comparison. Table 1 shows the details of the model used for both methods of testing, and Fig.2 shows the set-up of the model within the software.

Table 1 Details of the link and piezoelectric patch

Parameters	Link (Aluminium)	Piezoelectric Patch (PZT-5H)
Length (m)	0.4	0.056
Width (m)	0.035	0.028
Thickness (m)	0.003	0.0003
Density (kg/m^3)	2700	7500
Young's Modulus (GPa)	70	61.05
Piezoelectric coefficient, $\bar{e}_{31}$ (C/m^2)	N/A	-11

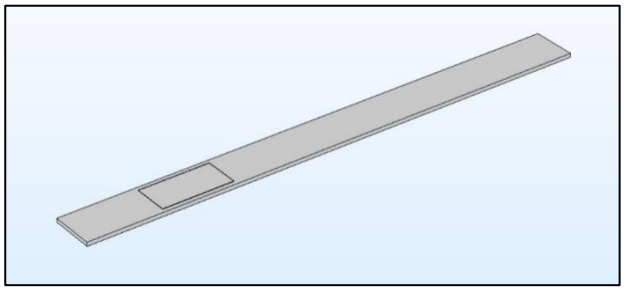

Fig. 2 COMSOL Multiphysics® model of link and bonded piezoelectric patches.

A free tetrahedral mesh was used on the COMSOL Multiphysics® model, and the maximum element size of this mesh was determined through a mesh convergence study. As can be seen in Fig.3 there was convergence observed when the maximum element size was around $0.02m$, this is very close to the predefined mesh size within the software 'Finer', was employed.

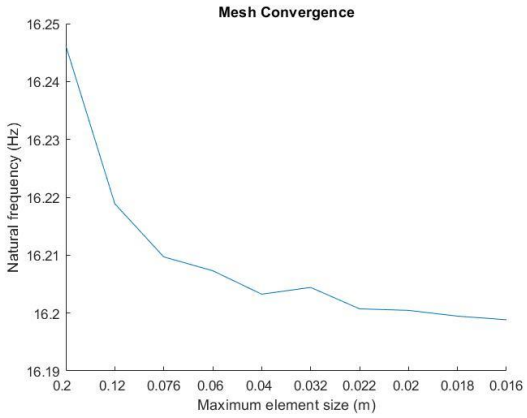

Fig. 3 Mesh convergence study on the first natural frequency of the beam.

The natural frequencies (ω_n) were calculated both analytically and through the COMSOL Multiphysics® model, with the first comparison not including the piezoelectric patches. The first three modes were tested, and the results are shown in Table 2.

Table 2 Natural frequency results for the first three modes

Mode	Analytical (H_z)	COMSOL® (H_z)	Error (%)
1	15.438	15.422	0.10
2	96.747	96.633	0.12
3	270.894	270.510	0.14

From the results, it is clear to see that the two modelling methods produce very similar natural frequencies. The error between the analytical and the COMSOL® results is expected due to two reasons; the link modelled analytically in two dimensions and modelled within COMSOL® in three dimensions, and that COMSOL® uses approximate numerical methods (such as FE) and the analytical method is more accurate.

For the second comparison, the analytical and simulation models were edited to include the two piezoelectric patches. The piezoelectric patches were set to a location along the beam (x_1) of 0.06m within both models. The natural frequencies retrieved from the two models are presented in Table 3 below.

Table 3 Natural frequency results for the first three modes (models include piezoelectric patches)

Mode	Analytical (H_z)	COMSOL® (H_z)	Error (%)
1	15.954	16.2	1.58
2	94.738	95.393	0.70
3	266.606	266.250	0.13

As can be seen from the results in Table 3 above, the inclusion of the piezoelectric patches produced slightly larger errors between the two different models for the first three modes. As the errors are all below three percent, the analytical model can be deemed as validated. The slight errors can, again, be explained by the reasons mentioned previously.

3 Active Vibration Control

3.1 Design of control system

A Proportional-Differential (PD) controller was implemented for the attenuation of the transverse motion of the link as a result of an initial displacement at the free end of the link. The control system took advantage of the indirect piezoelectric effect, so that the output of the system was the voltage to be applied across the piezo patches. Fig.4 below shows the model of the control system used.

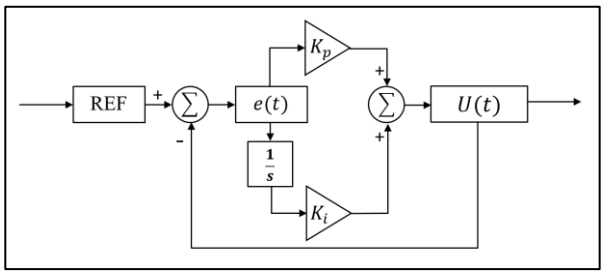

Fig. 4 Model of the PD Control system

The control model can be expressed as the following equation for use within the analytical model:

$$U(t) = K_p e(t) + K_d \frac{de(t)}{dt} \tag{15}$$

where, REF is the desired displacement of the tip of the link ($0\ m$), and $e(t)$ is the error, which is the difference between REF and the measured displacement. $U(t)$ is the controlled output of the system, which, in this instance is the displacement of the tip of the beam, and K_p and K_d are the proportional and differential gains, respectively. As the output of the control system is the displacement required for the attenuation of the vibration of the tip, and the voltages required to be applied across the two piezoelectric patches are to be obtained, the following equation is to be used.

$$V(t) = \frac{1}{2\chi_2}\left(M\frac{d^2U(t)}{dt^2}\right) \tag{16}$$

where, $V(t)$ is the total voltage required, M is the mass of the system, $U(t)$ is the controlled output of the system, and χ_2 is as follows:

$$\chi_2 = \frac{\bar{e}_{31}W}{2T_p}\left[\left(T_p + \frac{T}{2}\right)^2 - \frac{T^2}{4}\right] \times \left(\frac{dX_n(x_2)}{dx} - \frac{dX_n(x_1)}{dx}\right) \tag{17}$$

Although the operating voltage range of piezoelectric patches generally include negative voltages, the magnitude of the negative voltages is a lot smaller than the positive voltages i.e. a piezoelectric patch may have an operating voltage of -60V to 360V. Therefore, within this paper the operating voltage range will be considered to be positive only. The magnitude of the positive voltages obtained within equation 16 will be applied to the piezoelectric patch on the upper surface of the link, and the magnitude of the negative voltages will be applied to the piezoelectric patch on the lower surface of the link.

3.2 Analytical model of control system

To incorporate the control system into the analytical model, equation 13 is to be re-written so that it includes the control law $u(t)$ (which in this case represents force) as follows [9].

$$\ddot{T}_n(t) + 2\zeta\omega_n\dot{T}_n(t) + \omega_n^2 T_n(t) = u(t) \tag{18}$$

Writing the above equation in terms of the velocity and acceleration, so that the equations to be solved become second order differential equations, yields:

$$\begin{aligned} \dot{y}_1 &= y_2 \\ \dot{y}_2 &= -2\zeta\omega_n y_2 - \omega_n^2 y_1 + u \end{aligned} \tag{19}$$

where, y_1, $\dot{y}_1$ and $\dot{y}_2$ are the displacement, velocity and acceleration of the system, respectively. M is the mass of the system, and the control law u may now be defined as:

$$u = -ky = -\begin{bmatrix} k_p & k_d \end{bmatrix}\begin{bmatrix} y_1 \\ y_2 \end{bmatrix} \tag{20}$$

Using the above relation and writing equation 20 into the matrix form:

$$\dot{y} = \boldsymbol{F}y + \boldsymbol{G}u \tag{21}$$

yields:

$$\begin{bmatrix} \dot{y}_1 \\ \dot{y}_2 \end{bmatrix} = \begin{bmatrix} 0 & 1 \\ -\omega_n^2 & -2\zeta\omega_n \end{bmatrix}\begin{bmatrix} y_1 \\ y_2 \end{bmatrix} + \begin{bmatrix} 0 \\ 1 \end{bmatrix}u \tag{22}$$

The above equation (23) can then be used to produce the following equations to be solved to find the displacement and the velocity of the system (y_1 and y_2).

$$\begin{aligned} \dot{y}_1 &= y_2 \\ \dot{y}_2 &= -(\omega_n^2 + k_p)y_1 - (2\zeta\omega_n + k_d)y_2 \end{aligned} \tag{23}$$

To find the voltage required for the control the value of $U(t)$ can be calculated using the following equation.

$$U(t) = k_d y_2(t) + k_p y_1(t) \tag{24}$$

4 Parametric Study

4.1 Objective function

To obtain the best of both the location of the piezoelectric patches and the control gains an objective function was required. In this case this has been chosen to be the amount of time necessary to attenuate the displacement of the tip of the link to a value below an arbitrarily chosen displacement value (t_{Atten}). For the purpose of the optimisation this chosen displacement value will be referred to as the Effective Zero Displacement (EZD) value, any amplitudes of the displacement below this value will be considered to be zero. The EZD value is chosen based on when the tip displacement becomes acceptably attenuated (barely

noticeable to the naked eye); to allow the vibrations to stop completely would require a significantly greater amount of time.

The parametric study will focus on reducing t_{Atten} for the harmonic motion of the link, when subject only to an initial displacement at its free end. This initial displacement has been arbitrarily chosen as a value that a link within a robot system of the physical parameters within Table 1 is likely to be subject to. The viscous air damping coefficient (c_a) is taken to be 4.4 kg/s.

4.2 Location of the piezoelectric patches

The location of the piezoelectric patches along the link (x_1) affects both the natural frequency of the model, and the moment produced by the actuators on the beam. These two variables, in turn, effect the time taken to attenuate the amplitude of the vibrations below the EZD. For a range of actuator locations ($0.02: 0.001: 0.12$), set values of the gains ($K_p = 2$ and $K_d = 1s$), and an initial tip displacement of $0.01m$, t_{Atten} was obtained. The locations were limited to this range as in previous research the ideal location was proven to be nearest to the fixed end of the beam when the length of the piezoelectric patches was less than the length of the link [4]. The results are presented in Fig.5 below.

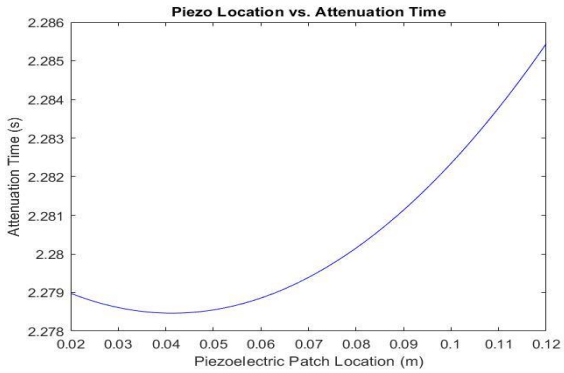

Fig. 5 Attenuation time for each location of the piezoelectric patches

The results show that for the dimensions and properties of the link and piezoelectric patches (see Table 1) the best location (x_1) lies around 0.04m. This is to be expected as the maximum strain energy is at the clamped end of the link.

4.3 Control gains

The proportional and differential control gains affect the voltage to be applied across the piezoelectric patches, thus affecting the moment the actuators produce upon the link. As both types of gains are used within the controller it was important to obtain the best values of the gains as a combination of K_p and K_d, so that for each value of K_p within a set range, a range of K_d values were used. This meant that for the proportional gain range of $0: 0.1: 60$, and a differential gain range of $0: 0.01: 4.4s$ there were 601x441 combinations of values tested.

An issue with acquiring the best combination of the gains is that most piezoelectric actuators will have a range for the operating voltage. In this case the operating voltage of the actuators was assumed to be 0 to 360V, and the maximum voltage produced for each combination of gains was recorded. Therefore, any gains which produced a voltage exceeding this operating voltage were eliminated. Although, it should be noted that the range of the gains tested were chosen to eliminate voltages above the maximum operating voltage of the piezoelectric patches to a certain extent.

The locations of the actuators were kept at a constant value throughout the optimisation of the gains ($x_1 = 0.04m$), and the tip of the link was subject to an initial displacement of $0.01m$. A small selection of the results is presented in Fig.6, note that the differential gain range has been reduced to improve the presentation.

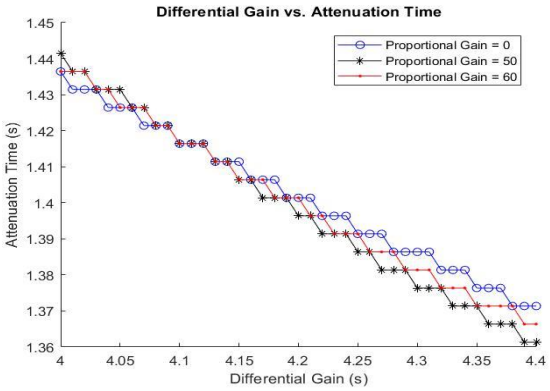

Fig. 6 Attenuation time against the proportional gain for three different proportional gain values.

The results show that as the differential gain is increased, the time required to attenuate the tip displacement below the EZD is reduced. The alteration of the proportional control value did not have as a significant effect on the attenuation time. However, as can be seen in the above figure, the best combination of gains (which still allow the maximum voltage required to lie within the operating voltage) is $K_p = 50$ and $K_d = 4.4s$.

5 Results

Once the best location of the piezoelectric patches and the best combination of control gains were found, the open and closed loop response of the system could be predicted through the analytical model. Fig.6 shows the open and closed loop response of the system when the dimensions and properties of the link and piezoelectric patches are those within Table 1, for the first mode of the model. The initial displacement at the tip of the link was set to 0.01m, and the free vibration of the tip of the clamped-free link as a result of the initial displacement was estimated. The location of the piezo patch and the control gains were the ideal values found through the parametric study ($x_1 = 0.04m$, $K_p = 50$ and $K_d = 4.4s$), and the viscous air damping coefficient (c_a) was set to 4.4 kg/s ($\zeta = 0.02$).

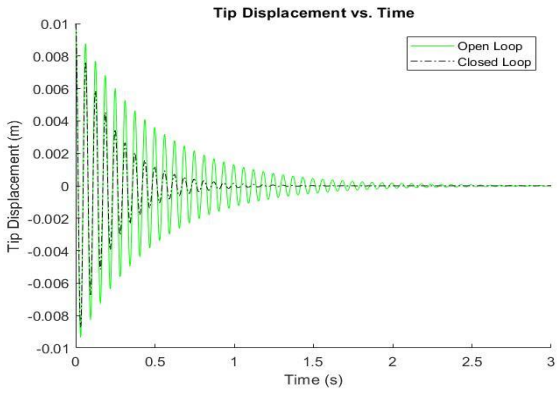

Fig. 7 The open and closed loop responses of the system over time

Fig.7 clearly shows that the closed loop response has a faster attenuation time compared to that of the open loop. Although some damping can be observed in the open loop response, which is due to the viscous air damping coefficient (c_a), the closed loop response can be seen to have a much greater damping.

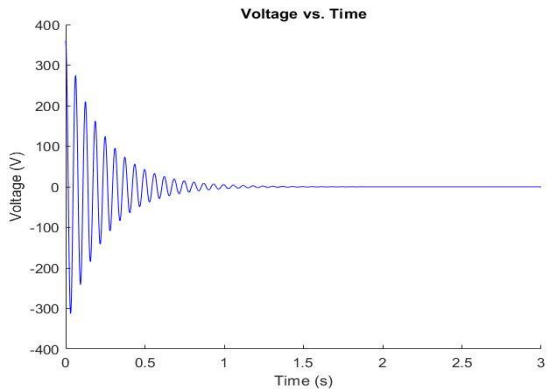

Fig. 8 The voltage applied across the upper and lower piezoelectric patches over time

The voltages that are to be applied across the piezoelectric patches can be seen within Fig.8. Here it can be seen that the maximum operating voltage of the piezoelectric patches is not exceeded. The magnitudes of the positive voltages are to be applied to the piezoelectric patch attached to the upper surface of the link, and negative to the patch attached to the lower surface.

6 Conclusion

This research has proven theoretically that the use of piezoelectric patches as actuators within AVC is an effective method of attenuated unwanted vibrations within a flexible link for the first mode. The modelling method of the link (EBT) has been validated through the use of a finite element model created using COMSOL Multiphysics®. A PD controller has been modelled analytically and has been effective at controlling the voltages to be applied across the actuators as a result of the free end displacement of the link. A parametric study was used to find the ideal variables, before the open and closed loop responses of the theoretical system were compared.

Although the research has proven theoretically that the proposed method for AVC is effective, the results have not been fully validated. Both the analytical models of the link with and without the inclusion of the piezoelectric patches have been proven to be accurate, through the comparison with the finite element model. However, it would then be necessary to verify the results produced through the use of AVC within the analytical model with results produced from a finite element model which also includes AVC.

The results of the research can then be validated further through the conduction of a physical experiment, which would be set up as the model in Fig.1. This research would include attempting to use low voltages (up to 50V) to power the piezoelectric patches for situations in which higher voltages are unobtainable, taking advantage of the negative operational voltages of piezoelectric patches. In order to fully comprehend and predict the vibrations experienced by a flexible link as part of a robot system future research would include a simulation of a robot arm with a flexible link attached to the end effector. It would then be possible to analyse the vibrations within the flexible link as a result of the motions of the robot arm, and eventually employ the AVC method used within this paper to attenuate said vibrations.

References

1 E.F.Crawley and J.Luis. AIAA Journal. *Use of Piezoelectric Actuators as Elements of Intelligent Structures*. **25**. 1373-1385. (1987).
2 V.Rathi and A.H.Khan. LAJSS. *Vibration attenuation and shape control of surface mounted, embedded smart beam*. **9, No. 3**. (2012).
3 K.A.M.Nor et al. IEEE Conference Publications. *Optimization in Active Vibration Control: Virtual Experimentation Using COMSOL Multiphysics – MATLAB Integration*. **5**. 385-389. (2014).
4 Q.Wang and C.M.Wang. IOPSCIENCE Journal. *Optimal placement and size of piezoelectric patches on beams from the controllability perspective*. **9**. 558-567. (2000).
5 H.Salmasi et al. CAODIE. *Active Vibration Suppression of a Flexible Link Manipulator Using a Piezoelectric Actuator*. **X**. 199-208 (2007).
6 Inman, D. J. (2014). *Engineering vibration*.
7 Erturk, A., & Inman, D. J. (2011). *Piezoelectric energy harvesting*. John Wiley & Sons.
8 H.Madinei et al. MSSP Journal. *Design of MEMS piezoelectric harvesters with electrostatically adjustable resonance frequency*. **81**. 360-374. (2016).
9 Bolton, W. (2002). *Control systems*. Newnes.